Renormalization group approach to a quasi-one-dimensional conductor with a triclinic band structure

August 9, 2020

Abstract

This part of the thesis project is concerned with the theoretical understanding of the phase diagram of the Bechgaard salts series by the renormalization group method. The full triclinic electron spectrum, as it can be obtained from density functional theory, will be implemented in the one-loop renormalization group calculations in order to describe the spin-density-wave to superconducting sequence of instabilities of the interacting electron gas as a function of applied pressure. The Lindhard or density-wave response function, which is an essential part of the renormalization group flow equations, has to be first evaluated and studied near the best nesting vector for both orthorhombic and triclinic band structure models.

1 Introduction

1.1 The Bechgaard salts as organic molecular crystals

The $(TMTSF)_2X$ (X = PF_6, AsF_6, ClO_4, ...) series of organic molecular crystals, also known as the Bechgaard salts series [1, 2], are nearly or quasi one-dimensional systems. They consists of chains of organic flat TMTSF [tretamethyltetraseleno-fulvalene] molecules [see Fig. 1 (a)] aligned along the parallel a direction and separated by anion sheets X[1]. The molecules essentially retain their flat shape in the solid state, so that the π type molecular orbitals, also called the highest occupied molecular orbitals (HOMO) of the TMTSF molecule, have their highest overlap preferentially along the a direction. The corresponding $\pi-$molecular overlap along the two transverse $\overrightarrow{OB}$ and $\overrightarrow{OC}$ directions shown in Fig. 1 are smaller by order of magnitudes. This is the main reason why these are close realizations of one-dimensional systems.

From X-ray crystallographic studies, the chains are not uniform and are slightly dimerized with a shorter and a longer distances between molecules. The result of this dimerization is to 'double' the unit cell of the crystal, which effectively consists of two TMTSF molecules and one anion X [see Fig. 1]. The crystal structure is triclinic with angles that differ from 90°.

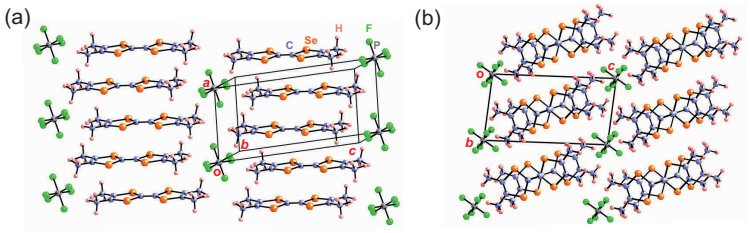

Figure 1: The crystal structure of the Bechgaard salts $(TMTSF)_2X$. Side (left) and top (right) views. From Guster et al. [3].
.

1.2 Electronic structure

The molecular TMTSF unit contains many carbon, selenium and hydrogen atoms, each of them consisting of many electrons. Correspondingly, the number of electron bands is expected to be very large. However, it turns out that the HOMO is essentially the only relevant orbital at low energy that crosses the Fermi level. Different approaches to band calculations (Extended Huckel[4, 5], density functional theory (DFT)[3] ...) confirms this. In Figure 2 (a), for instance, we reproduce the band structure of a compound like $(TMTSF)_2PF_6$. From the Figure we verify that within a width in energy of about 1 eV, only one

[1]The role of anions X is to assure a so-called charge transfer in the solid state: the anion X captures one electron coming from two TMTSF molecules. The partially emptied HOMO π orbitals make then possible the existence of a metal for these systems.

band is present and crosses the Fermi level at energy zero. Note that here the presence of a small dimerization opens a gap in the middle of the band at points X and M in Fig. 2 (a). This dimerization gap makes the band effectively half-filled.[2]

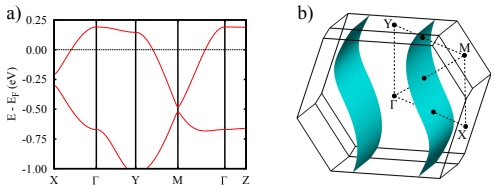

Figure 2: DFT band structure calculations (a) and the corresponding open Fermi surface (b) for the triclinic $(TMTSF)_2X$. From [3]

1.3 The phase diagram

Resistivity measurements confirm the existence of a metallic state in normal (ambient) pressure and temperature conditions for the Bechgaard salts. However, when cooled down, phase transitions take place indicating a collective behavior for the whole electron system. For instance, at low pressure, the system undergoes a sharp metal-insulator transition near $T_{SDW} \sim 10$ K with a gap that opens at the Fermi level. According to several other experiments (susceptibility, NMR, EPR, etc.), it is firmly established that the nature of the transition is magnetic in character and consists with a spin-density-wave ordered state of modulation wave vector $\boldsymbol{q}_0$[1, 2].

When pressure is applied, T_{SDW} undergoes a gradual decrease that becomes critical at the approach of a critical pressure. Instead of touching zero, the system becomes a superconductor at $T_c \sim 1$K [6], which in its turn undergoes a gradual decrease [see Fig. 3] [7]. It follows that a 'superconducting dome' is formed, which is typically found in many unconventional superconductors (cuprates, pnictides, heavy fermions, etc. See Ref.[8])[3]. The characteristic sequence SDW $\rightarrow$ SC under pressure also stands out as a clear example of quantum criticality emerging for the interplay from two ordered states.

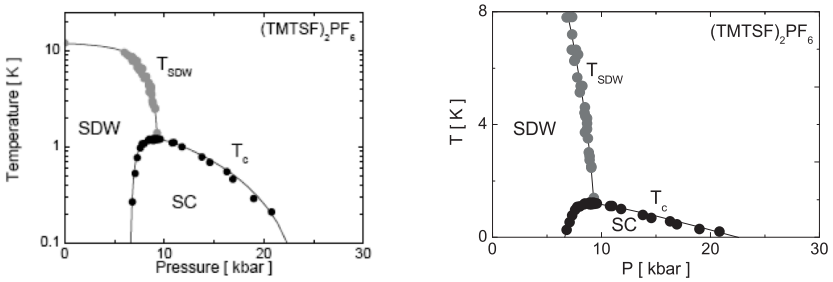

Figure 3: Phase diagram $(TMTSF)_2PF_6$ under pressure on a semi-logarithmic scale (a) and linear scale near the quantum critical point (b). SDW stands for spin-density-wave state and SC for superconductivity. From [7].

1.4 Triclinic and approximate orthorombic electron spectrum

Triclinic tight-binding electron spectrum In the triclinic structure, the angles between the crystallographic axis differ from 90°; furthermore, possibilities of overlap along the transverse b direction are multiple, as can be seen in Figure 4. According to the work of Yamaji [9] and also Hasegawa and Kishigi[10], the tight-binding quasi-1D spectrum of $(TMTSF)_2X$, which is compatible with the triclinic structure, can be put in the following form:

$$\epsilon^p_{\boldsymbol{k}} = v_F(pk - k_F) + \epsilon^p(k_\perp) \tag{1}$$

where $p = \pm$ is the branch index for right (+) and left (−) moving carrier, v_F their longitudinal velocity, and k_F is the 1D Fermi wave vector in the absence of $\epsilon^p_\perp$. As for the transverse part of the spectrum, it can be written in series form

[2]From a purely stochiometric viewpoint, that is, by neglecting dimerization, the $(TMTSF)_2X$ compound should have 1/2 hole per TMTSF molecule and the band would be 3/4 filled. In presence of dimerization, a gap opens not at the Fermi level, but in the middle of the 3/4 filled band, which splits into one filled and one half-filled band (see Fig. 2 (a)).

[3]The superconducting dome following an antiferromagnetic ordered state in the Bechgaard salts is apparently the first to have been discovered in unconventional superconductors.

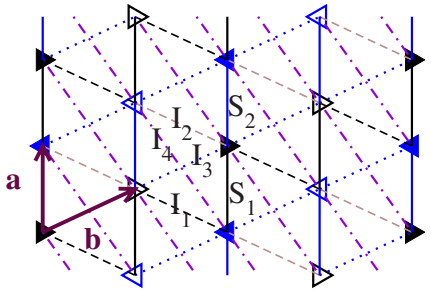

Figure 4: Possibilities of orbital overlaps in the ab plane of $(TMTSF)_2X$ in their triclinic structure. From [10].

$$\begin{aligned}\epsilon^p(k_\perp) = &-2t_b\cos(k_\perp - p\phi)\\ &-2t'_\perp\cos[2(k_\perp - p\phi)b] - p2\tau'_\perp\sin[2(k_\perp - p\phi)]\\ &+\ldots\end{aligned} \tag{2}$$

where $t_\perp$ is the first nearest-neighbor interchain hopping; $t'_\perp$ and $\tau'_\perp$, etc., are next-nearest neighbor interchain hopping terms compatible with the triclinic structure. The angle ϕ ($\geq -\pi/2$) can be connected to overlap integrals of the triclinic structure; its value varies for compound to compound, namely for different anion X. Here

$$k \equiv \boldsymbol{k}\cdot\boldsymbol{a}, \quad k_\perp \equiv \boldsymbol{k}\cdot\boldsymbol{b}.$$

where $\boldsymbol{a}$ and $\boldsymbol{b}$ are the lattice vectors of the ab plane in the triclinic cell. The expression for $\epsilon^p_{\boldsymbol{k}}$ in (1-2) gives an excellent fit of the DFT spectrum of Fig. 2 (a).

The triclinic spectrum has well defined nesting properties at some nesting vector that will be called $\boldsymbol{q}^t_0$. For instance, when next to nearest neighbor hopping terms $t'_\perp$ and $\tau'_\perp$ are zero, one has the electron-hole symmetry relation:

$$\epsilon^+_{\boldsymbol{k}+\boldsymbol{q}^t_0} = -\epsilon^-_{\boldsymbol{k}} \tag{3}$$

where according to (1-2), is satisfied for the nesting vector

$$\boldsymbol{q}^t_0 = (2k_F, \pi + 2\phi) \tag{4}$$

at $t'_\perp = \tau'_\perp = 0$. Now when both $t'_\perp \neq 0$ and $\tau'_\perp \neq 0$, deviations are found and $\epsilon^+_{\boldsymbol{k}+\boldsymbol{q}^t_0} \neq -\epsilon^-_{\boldsymbol{k}}$.

Orthorombic approximation If we now focus on the simpler orthorhombic approximation for the spectrum for which a square lattice is considered in the ab plane, where $\boldsymbol{a} \perp \boldsymbol{b}$ are at right angles. This is the most common approximation of the spectrum used. In this case, the tight-binding spectrum (with respect the Fermi energy ϵ_F) reads

$$\epsilon_{\boldsymbol{k}} = -t_a\cos ka - 2t_\perp\cos k_\perp - \epsilon_F \tag{5}$$

where t_a and $t_\perp$ are the intrachain and interchain hopping integrals. If we look at the equation for the Fermi surface $\boldsymbol{k}_F = (k_F(k_\perp), k_\perp)$, we use the condition $\epsilon_{\boldsymbol{k}_F} = 0$ for (5), which gives two ($p = \pm$) warped Fermi sheets

$$\begin{aligned}k^p_F(k_\perp) = &\ p\arccos\left(\frac{-\epsilon_F}{2t_a} - \frac{t_\perp}{t_a}\cos k_\perp\right)\Bigg|_{t_\perp/t_a \ll 1}\\ \simeq &\ p[k_F - \frac{1}{v_F}\epsilon^0_\perp(k_\perp)]\end{aligned} \tag{6}$$

where

$$\epsilon^0_\perp(k_\perp) = -2t_\perp\cos k_\perp - 2t'_\perp\cos 2k'_\perp + \ldots \tag{7}$$

Here $v_F = 2t_a\sin k_F + \ldots$ is the longitudinal velocity and $t'_\perp, \ldots$ are different harmonics of interchain hopping generated by the expansion of (6) at small $t_\perp/t_a$. These effective interchain hopping between second, ... neighbors chains introduce frustration in the nesting properties of the spectrum.

The Fermi sheets in this approximation are plotted in Figure 5 (compare with those of Fig. 2 (b) for the triclinic case). The

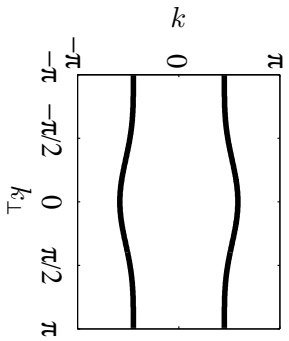

Figure 5: Quasi-one-dimensional open Fermi surface for a square lattice in the ab plane.

linearized spectrum around the Fermi sheets then takes the form:

$$\begin{aligned}\epsilon^p_{\boldsymbol{k}} &\simeq v_F[pk - k^p_F(k_\perp)] \\ &= v_F(pk - k_F) + \epsilon^0_\perp(k_\perp)\end{aligned} \tag{8}$$

In the absence of $t'_\perp$, $\epsilon^0_\perp(k_\perp) \to -2t_\perp \cos k_\perp b$ and there is perfect nesting properties at

$$\boldsymbol{q}_0 = (2k_F, \pi)$$

which corresponds to an electron-hole symmetry in the spectrum at $t'_\perp = 0$. The latter takes the form

$$\epsilon^+_{\boldsymbol{k}+\boldsymbol{q}_0} = -\epsilon^-_{\boldsymbol{k}}. \tag{9}$$

When $t'_\perp \neq 0$, there are deviations which read

$$\epsilon^+_{\boldsymbol{k}+\boldsymbol{q}_0} = -\epsilon^-_{\boldsymbol{k}} + 4t'_\perp \cos 2k_\perp \tag{10}$$

We note that only few points of perfect nesting remain and these occur at $k_\perp = \pm\pi/4, \pm 3\pi/4$.

2 Parameters

In the following, we shall specify the range of parameters to be used in the one-loop RG with 3 independent transverse variables. First, one can recall the phase diagram already obtained by the RG in the orthorhombic limit, namely at $\tau = 0$, $\phi = 0$ [11], which is shown in Fig. 6.

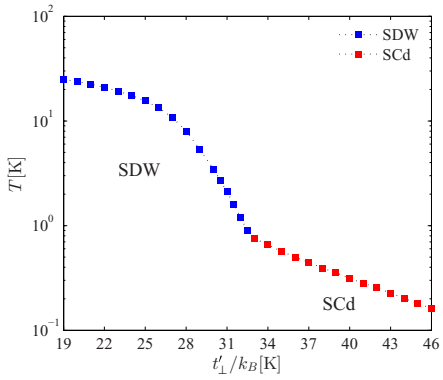

Figure 6: Phase diagram in the orthorhombic limit for a square lattice in the ab plane. From the work of [11], the band structure parameters used are $E_F = 3000$K, $t_\perp = 200$K, and $g_1 = 0.32 \approx g_2/2$, $g_3 \approx 0.025$ are the normalized bare coupling constants.

2.1 RG Susceptibilities

The temperature scale at which each instability occurs is determined by the temperature where a singularity occurs in the μ =SDW or SCd susceptibility, namely:

$$\tilde{\chi}_\mu(\boldsymbol{q}_\mu) = 2\int_0^\infty \langle z_\mu^2(k_\perp)\mathcal{I}_\mu(k_\perp, q_\mu)\rangle_{k_\perp} d\ell, \tag{11}$$

where $z_\mu(k_\perp)$ is the renormalization factor for the source-pair vertex. It obeys the flow equation

$$\partial_\ell z_\mu(k_\perp) = \frac{1}{2}\langle f_\mu(k'_\perp) g_\mu(\bar{k}'_\perp)\mathcal{I}_\mu(k_\perp, k'_\perp, q_\mu)\rangle_{k'_\perp}. \tag{12}$$

Here the on-shell Peierls ($\nu = P$) and Cooper ($\nu = C$) loops at finite T in (12) are given by [12]

$$\begin{aligned}\mathcal{I}_\nu(k'_\perp, k_\perp, q_\nu) = {} & \frac{\Lambda(\ell)}{2}\sum_{\lambda=\pm1}\int_{k'_\perp-\frac{\pi}{N_P}}^{k'_\perp+\frac{\pi}{N_P}}\frac{dk'_\perp}{2\pi} \\ & \times \frac{\theta(|\Lambda(\ell)+\lambda A_\nu| - \Lambda(\ell))}{2\Lambda(\ell)+\lambda A_\nu} \\ & \times \Big[\tanh[\beta\Lambda(\ell)/2] + \tanh[\beta(\Lambda(\ell)/2 + \lambda A_\nu/2)]\Big].\end{aligned} \tag{13}$$

Here $\theta(x)$ is the Heaviside function [$\theta(0) \equiv \frac{1}{2}$], and

$$\begin{aligned}A_\nu(k_\perp, k'_\perp, q_\nu) = {} & -\epsilon_\perp^-(k'_\perp) - \eta_\nu\epsilon_\perp^+(\eta_\nu k'_\perp + q_\nu) \\ & + \eta_\nu\epsilon_\perp^+(\eta_\nu k_\perp + q_\nu) + \epsilon_\perp^-(k_\perp),\end{aligned} \tag{14}$$

for which $\eta_{P,C} = \pm1$ for the Peierls and Cooper channel respectively. The expression for $\epsilon_\perp^{p=\pm}$ is given by (2). *We presume that the bubble $\mathcal{I}_\mu(k_\perp, q_\mu)$ appearing in (11) for χ_μ can be obtained from (14) by putting $k_\perp = k'_\perp$ (?).*

2.1.1 Spin-density-wave case

Considering SDW in the general case, the susceptibility $\tilde{\chi}_{\rm SDW}(\boldsymbol{q}_{\rm SDW})$ is the one evaluated at the best nesting vector (Eq. 4):

$$\boldsymbol{q}_{\rm SDW} \equiv \boldsymbol{q}_0^t = (2k_F, \underbrace{\pi + 2\phi}_{q_P}),$$

which depends on the shift angle ϕ. We have

$$A_{\rm SDW}(k_\perp, k'_\perp, \pi + 2\phi) = -\epsilon_\perp^-(k'_\perp) - \epsilon_\perp^+(k'_\perp + \pi + 2\phi) + \epsilon_\perp^+(k_\perp + \pi + 2\phi) + \epsilon_\perp^-(k_\perp), \tag{15}$$

The corresponding combination of couplings for SDW is

$$g_{\rm SDW}(\bar{k}'_\perp) = g_2(k'_\perp + \pi + 2\phi, k_\perp, k_\perp + \pi + 2\phi) + g_3(k'_\perp + \pi + 2\phi, k_\perp + \pi + 2\phi, k'_\perp) \tag{16}$$

whereas the form factor for the SDW order parameter susceptibility is

$$f_{\rm SDW}(k'_\perp) = 1. \tag{17}$$

2.1.2 Superconducting d-wave case

If we now turn to the superconducting d-wave case, the corresponding susceptibility $\tilde{\chi}_{\rm SCd}(\boldsymbol{q}_{\rm SCd})$ is evaluated at the wavevector

$$\boldsymbol{q}_{\rm SCd} = 0$$

which in the general triclinic case still refers to the (zero) momentum of Cooper pairs which is independent of the shift angle ϕ.

In the loop expression for the SCd situation, we have according to (14)

$$A_{\rm SCd}(k_\perp, k'_\perp, q_{\rm SCd} = 0) = -\epsilon_\perp^-(k'_\perp) + \epsilon_\perp^+(-k'_\perp) - \epsilon_\perp^+(-k_\perp) + \epsilon_\perp^-(k_\perp) \equiv 0, \tag{18}$$

and for which, following (2), the terms cancel each other. The loop $\mathcal{I}_C$ of Cooper pair vertices, when evaluated at zero pair momentum, is then independent of $k_\perp$ and $k'_\perp$. This is consistent with the logarithmic singularity of the loop (13) for a general spectrum having the inversion symmetry property $\epsilon^p(\boldsymbol{k}) = \epsilon^{-p}(-\boldsymbol{k})$.

As for the combination of coupling constants relevant to SCd, we have

$$g_{\rm SCd}(\bar{k}'_\perp) = -g_2(k'_\perp, -k'_\perp, k_\perp) - g_1(k'_\perp, -k'_\perp, k_\perp). \tag{19}$$

Finally the d-wave form factor in (12) for the general triclinic case,

$$f_{\rm SCd}(k_\perp) \to f^p_{\rm SCd}(k_\perp) = \sqrt{2}\cos(k_\perp - p\phi), \tag{20}$$

which carries a branch dependence in order to assure even parity of the d-wave spatial part of the order parameter ($f^p_{\rm SCd}(k_\perp) = f^{-p}_{\rm SCd}(-k_\perp)$). However the end result (average over $k_\perp$) is of course independent of p. The dependence on ϕ will introduce a shift in the zero's of the superconducting gap. Recall that for $\phi = 0$, the nodes of the gap are at $k_\perp = \pm\pi/2$, these positions will differ at $\phi \neq 0$.

2.1.3 Range of parameters

Besides the above values of the parameters entering in the RG calculations E_F, $t_\perp$, and the bare $g_{1,2,3}$, we will take for the transverse part of the spectrum [9],

$$\tau'_\perp = -t'_\perp/2 \tag{21}$$

where $t'_\perp$ falls in the interval of the one given in Fig. 6. As for the angle ϕ, according to band calculations of Ref. [9], it should fall in the interval $\phi \in [-2\pi/5, 0]$. For example, on can try the three values:

$$\phi = 0, -\pi/8, -\pi/4, \tag{22}$$

where $\phi = 0$ is a test value for recovering old results (note that old results in Fig. 6 were obtained for $\tau'_\perp = 0$).

References

[1] K. Bechgaard et al., Solid State Comm. **33**, 1119 (1980).

[2] D. Jérome and H. J. Schulz, Adv. Phys. **31**, 299 (1982).

[3] B. Guster, M. Pruneda, P. Ordejon, E. Canadell, and J. P. Pouget, preprint (2019).

[4] P. M. Grant, J. Phys. Colloq. **44**, C3 847 (1983).

[5] L. Ducasse, A. Abderrabba, and B. Gallois, J. Phys. C **18**, L947 (1985).

[6] D. Jérome, A. Mazaud, M. Ribault, and K. Bechgaard, J. Phys. (Paris) Lett. **41**, L95 (1980).

[7] N. Doiron-Leyraud et al., Phys. Rev. B **80**, 214531 (2009).

[8] L. Taillefer, Annu. Rev. Condens. Matter Phys. **1**, 51 (2010).

[9] K. Yamaji, J. Phys. Soc. Jpn. **55**, 860 (1986).

[10] Y. Hasegawa and K. Kishigri, Phys. Rev. B **81**, 235118 (2010).

[11] M. Shahbazi and C. Bourbonnais, Phys. Rev. B **94**, 195153 (2016).

[12] M. Shahbazi et al., Phys. Rev. B **95**, 165111 (2017).